coatings

MDPI

Article

Processing and Weathering of Sol-Gel Clearcoats for Coil-Coated Steel

Evan Watkins [1,*], Chris Griffiths [2], Chris Batchelor [2], Peter Barker [3] and Matt Carnie [1,2]

[1] Materials Research Centre, Faculty of Science and Engineering, Swansea University, Bay Campus, Fabian Way, Swansea SA1 8EN, UK; m.j.carnie@swansea.ac.uk
[2] Sustainable Product Engineering Centre for Innovative Functional Industrial Coatings (SPECIFIC), Faculty of Science and Engineering, Swansea University, Bay Campus, Fabian Way, Swansea SA1 8EN, UK; c.m.griffiths@swansea.ac.uk (C.G.); c.p.batchelor@swansea.ac.uk (C.B.)
[3] Tata Steel UK, Shotton Works, Deeside CH5 2NH, UK
* Correspondence: 2029383@swansea.ac.uk

Abstract: Clearcoats provide long-term aesthetics and protection for underlying coating systems, increasing product lifetimes. However, organic clearcoats are predominantly produced using fossil-fuel feedstocks. In search of a sustainable alternative, an experimental investigation was conducted on the development of glass-like clearcoats produced using the sol-gel process. The processing of sol-gel clearcoats over a pigmented polyurethane coating was studied by modifying the sol-gel solution pH, ageing, curing, precursor chemistry and deposition techniques. Under optimal formulation and processing conditions, defect-free sol-gel clearcoats were produced that have the potential to be scaled up to a coil-coating line using existing technologies. Mechanical testing demonstrated the coatings had excellent adhesion, hardness, and flexibility. Furthermore, accelerated laboratory weathering tests revealed the sol-gel coatings had superior degradation resistance compared to the organic coatings tested, resulting in negligible colour changes and higher gloss retention after 4000 h of exposure. The durability and environmental benefits of sol-gel clearcoats highlight their potential as a replacement for traditional organic clearcoats in a variety of applications.

Keywords: glass clearcoats; sol-gel process; organic-inorganic hybrids; weathering; degradation; coil-coating; sustainability

Citation: Watkins, E.; Griffiths, C.; Batchelor, C.; Barker, P.; Carnie, M. Processing and Weathering of Sol-Gel Clearcoats for Coil-Coated Steel. *Coatings* **2023**, *13*, 982. https://doi.org/10.3390/coatings13060982

Academic Editors: Zuoli He and Ivan Jerman

Received: 5 May 2023
Revised: 19 May 2023
Accepted: 23 May 2023
Published: 25 May 2023

1. Introduction

Organic clearcoat systems have long been used to enhance the durability and resistance to environmental degradation of building materials exposed to the outdoors [1]. These systems maintain the long-term aesthetics of the materials, such as gloss retention and minimal colour change (ΔE), while providing a barrier to the underlying coating systems [2]. However, organic coatings are derived from non-renewable fossil-fuel sources. Renewable alternatives currently require further development before they can match the performance and manufacturing costs of fossil-fuel-derived coatings [3]. In search of a more sustainable alternative, the sol-gel process for producing glassy/ceramic coatings as a durable clearcoat system is being explored.

The sol-gel process to produce glassy/ceramic coatings has been well documented in the literature for metal substrates as durable barrier coatings and for functional applications such as photocatalysis [4–7]. However, there is less research on the use of sol-gel coatings on organic substrates, possibly due to issues reported, such as low thicknesses, defects and a material mismatch that can result in poor adhesion [8,9]. As well as material compatibility issues, there are also processing considerations. Most of the literature is based on thin film deposition technologies such as dip and spin-coating, which limits the industrial scalability of the sol-gel process [10,11]. Furthermore, the curing of sol-gel coatings is typically carried out at very high temperatures, which would cause thermal degradation of

polymeric substrates, or for long curing durations, which limits industrial scalability [12,13]. A solution to the defects that occur in sol-gel systems based upon tetraethoxysilane (TEOS) is to use organic-inorganic hybrid (OIH) coatings that consist of an organic component that results in improved flexibility [11,14].

Manufacturing coatings via a sol-gel process can have environmental benefits such as reduced processing times and energy requirements, can use non-toxic chemistries, and are often produced via scalable one-pot reactions [15–17]. Additionally, sol-gel coatings are typically an order of magnitude thinner than organic coating systems, resulting in VOC, CO_2 and material reductions. These factors, combined with the competitive costs of the abundant silica precursors, ensure that sol-gel coatings can compete with organic clearcoat systems [16].

The sol-gel precursors TEOS and methyltriethoxysilane (MTES) have been widely studied to understand the effects of utilising an organic component in the sol-gel network [18]. These precursors have been shown to produce coatings with varied mechanical properties and durability [4,19]. The sol-gel precursor isobutyltriethoxysilane (IBTES) incorporates a longer alkyl chain into the sol-gel network. This precursor was studied to understand the effects of using the longer alkyl chain OIH as a coating material.

This study evaluates the use of sol-gel coatings made from the precursors TEOS, MTES and IBTES on a pigmented polyurethane coating. The structures of the sol-gel precursors are depicted in Figure 1.

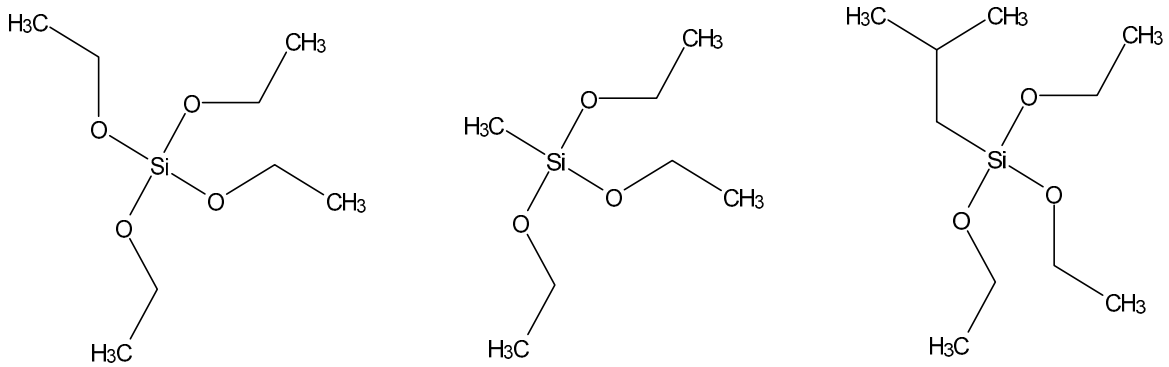

Figure 1. Chemical structures of the sol-gel precursors: TEOS (**left**), MTES (**middle**) and IBTES (**right**).

This work investigates the industrial feasibility of using novel sol-gel coatings to replace conventional organic clearcoats for coil-coated steels. Sol-gel coatings can be produced more sustainably at a lower cost whilst offering optimal mechanical properties and excellent durability to environmental degradation compared to organic clearcoats. The sol-gel coatings were applied to a pigmented polyurethane substrate. Processing parameters such as sol-gel solution ageing time, pH and coating thickness were varied, and the resultant inorganic TEOS coatings were evaluated and compared. A systematic study was implemented to determine the industrial suitability of TEOS and OIH-coated polyurethane. The ability to produce defect-free sol-gel coatings over polyurethane without activation of the polymer surface was studied, as this would be inhibitive to industrial scale-up. The mechanical properties of the coatings were determined to evaluate their suitability for coil coating. The weathering performance and degradation of the coatings when exposed to accelerated laboratory weathering testing were analysed and compared to that of a commercial polyurethane and polyurethane clearcoat, to understand how the durability of the sol-gel coating compares.

2. Materials and Methods

2.1. Materials

Concentrated HCl acid (37% conc.), tetraethoxysilane (TEOS) and isobutyltriethoxysilane (IBTES) were purchased from Sigma Aldrich, and ethanol was purchased from

Fisher Scientific, Hampton, VA, USA. Methyltriethoxysilane (MTES) was purchased from Fluorochem, Hadfield, UK. All chemicals used were of reagent grade. Hot-dipped galvanised (HDG) steel was provided by Tata Steel, Port Talbot, UK. A commercial pigmented polyurethane coating system and polyurethane clearcoat were used for testing and comparing the performance of the sol-gel coatings.

2.2. Methods

2.2.1. Coating Production

The TEOS-based sols were prepared by first mixing TEOS and ethanol for 10 min before adding HCl and water and then allowing the reaction to continue at ambient temperature for 1 h with continuous magnetic stirring. The molar ratio of all sols was fixed at 1:5.33:4:x (TEOS:ethanol:water: HCl). The concentration of the catalyst was varied to cover a range of pH values from ~0 to 5 by varying the molar ratio of HCl relative to TEOS (0.07, 0.02, 0.007, 0.002 and 0.0007). In order to evaluate the effect of ageing time on coating delamination, the coatings were deposited at ageing times of 0, 1, 2, 3, 7, 14, 21 and 28 days. The hybrid precursors MTES and IBTES were prepared in the same way as the TEOS coatings but utilised an HCl molar ratio of 0.002 and had an ageing time of 1 day.

2.2.2. Processing

HDG steel and pigmented polyurethane-coated steel were the substrates used for coating deposition. The substrates were cleaned using ethanol before the TEOS coatings were deposited using dip-coating (PTL-MM01, MTI Corporation, Richmond, VA, USA). The withdrawal speed used for the deposition process was 100 mm/min and 200 mm/min. After deposition, the TEOS coatings were cured in a convection oven at a peak metal temperature (PMT) of 210 °C for 12 min.

Fourier transform infrared spectroscopy (FTIR) was used to characterise the changes in sol-gel coating chemistry over time. However, when analysing the sol-gel coated polyurethane surface, the FTIR response was primarily from the polyurethane substrate due to the low coating thickness of the sol-gel. Therefore, the sol-gel coatings were applied to HDG steel surfaces for characterisation via FTIR as the signal response was far greater and changes in the sol-gel were easily visible.

Polyurethane-coated steel surfaces were subjected to plasma treatment using a Zepto plasma lab system (Diener Electronics, Ebhausen, Germany). The samples were cleaned using ethanol to remove surface contamination, dried and then placed into the plasma chamber. The chamber was pumped to a vacuum of 0.1 bar, filled with an oxygen atmosphere and then the plasma was activated for one minute before the samples were removed and the sol-gel coating was applied.

Hybrid sol-gel coatings were deposited using bar and spray coating, then cured using a convection oven, achieving a PMT of 232 °C over 45 s. The bar-coated samples were deposited using a 6 µm K-bar. The spray-coated samples were deposited using a modified ultrasonic spray rig (MSK-USP-ST1, MSK-SP-01A, MTI Corporation, Richmond, VA, USA). The ultrasonic nozzles were operated at a frequency of 40 kHz at 130 W with a nozzle height of 3 cm from the sample surface.

The effect of temperature and time on the cure and densification of the sol-gel coatings was achieved through a systematic study. Samples were cured at a range of PMTs (room temperature (RT), 100 °C, 150 °C, 200 °C and 232 °C) and times (45 s and 12 min) using sols at pH 4 and allowing for 24 h of ageing. A PMT of 232 °C for 12 min was not utilised due to the degradation of the polyurethane substrate. Table 1. highlights the curing parameters used in this study.

Table 1. Curing parameters studied.

Peak Metal Temperature (°C)	Curing Duration
RT	-
100	45 s 12 min
150	45 s 12 min
200	45 s 12 min
232	45 s

2.2.3. Characterisation and Laboratory Weathering Techniques

The surface morphology of the coatings was visualised using digital microscopy (Keyence VHX-7000, Osaka, Japan). Coating thickness was measured using scanning electron microscopy (SEM)(Hitachi, TM3000, Tokyo, Japan). The wettability of the surface was determined using a contact angle goniometer (Osilla) and measuring the water contact angle (WCA) in contact with the coating surfaces. Three measurements across each sample were taken. The surface roughness was measured using a handheld profilometer (Taylor Hobson Surtronic S-128, Leicester, UK) with an accuracy of ±10 nm. Three measurements across each sample were taken. Attenuated total reflectance Fourier transform infrared spectroscopy (ATR-FTIR)(PerkinElmer spectrum 100, Waltham, MA, USA) with a Specac ATR attachment was utilised to characterise the structures of the coatings. Spectra were collected in transmittance mode with 8 scans at a 4 cm^{-1} resolution in the wavelength range of 4000–500 cm^{-1}. L*a*b* CIE Labs colour measurements were carried out using a spectrophotometer (X-Rite Handheld Sphere Ci 60 Series, Grand Rapids, MI, USA). By using the L*a*b* values, the colour change (ΔE) was calculated using Equation (1). [20]

$$\Delta E = \sqrt{(L_1 - L_0)^2 + (a_1 - a_0)^2 + (b_1 - b_0)^2} \quad (1)$$

Gloss measurements were taken at a projecting angle of 60°, and the glossmeter was calibrated using a standard of known gloss units before the measurement of the samples. Three measurements across each sample were taken. The gloss retention was calculated using Equation (2) [21].

$$\text{Gloss retention } (\%) = \left(\frac{\text{Gloss}}{\text{Initial Gloss}}\right) \times 100 \quad (2)$$

The qualitative mechanical properties of the coating systems were analysed according to the coil-coating standards for pencil hardness [22], cross-hatch adhesion [23] and T-bend mandrel testing [24].

A QUV accelerated weathering tester (Q-Lab QUV/se) was utilised to simulate outdoor weathering on the coated samples. The testing was performed to the standard EN 13523-10 [25]. Samples were cycled through periods of 4 h of dry UV exposure at a black panel temperature of 60 °C, followed by a period of 4 h of water condensation exposure without radiation at a black panel temperature of 40 °C. Two samples per coating were subjected to testing.

3. Results and Discussion

3.1. FTIR-ATR Spectroscopy

The structure of the resultant coatings when utilising the precursors TEOS, MTES and IBTES was evaluated using FTIR Spectroscopy. The FTIR spectra are shown in Figure 2. The characteristic vibrations of the bonds within each coating are shown in Table 2.

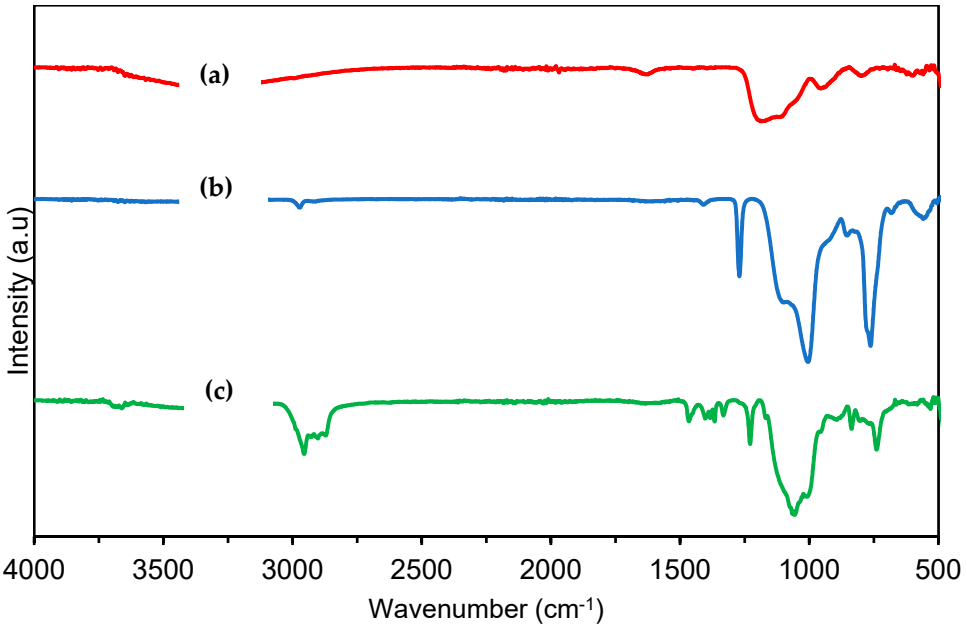

Figure 2. FTIR–ATR spectra of sol-gel coatings produced using the precursors: (**a**) TEOS, (**b**) MTES and (**c**) IBTES.

Table 2. Assignment of the bands from the FTIR-ATR spectra.

Wavenumbers (cm^{-1})	Vibrational Modes	References
3200–3400	O–H stretching	[26]
2970–2870, 1470–1330	C–H stretching	[27]
1630	O–H bending	[26]
1270–1230	Si–C stretching	[27]
1170–1000	Si–O–Si stretching	[26,28]
950	Si–OH bending	[26]
790	Si–O–Si bending	[29]
760–740	Si–C stretching	[27]
550	$Si–O^-$ rocking	[29]

The FTIR spectra of the coating systems varied due to the effect of the alkyl chain in the sol-gel network, which resulted in different reaction rates and final structures. The TEOS coating contains a broad peak at 3200–3400 cm^{-1} which corresponds to O–H species such as Si–OH and H_2O, which remain within the cured coating due to the slower reaction rates of this coating system [26]. The MTES coating contained a small peak at 2970 cm^{-1} that corresponded to C–H stretching due to the presence of $Si–CH_3$ within the cured coating. The IBTES coating contained several strong absorptions at 2960–2870 cm^{-1} that correspond to C–H stretches due to the isobutyl group within the coating [27]. Peaks were observed in the range 1470–1330 cm^{-1} in the MTES and IBTES coatings due to vibrations within the alkyl chains, characteristic of C–H bonds from CH_3, CH_2 and CH groups [27]. A sharp peak at 1270 cm^{-1} for MTES and 1230 cm^{-1} for IBTES corresponds to Si–C stretching [27]. The change in vibration for the Si–C absorption in the IBTES coating is potentially due to a weaker force constant due to electron density withdrawal through the isobutyl group [30]. The wavenumber region of 1170–1000 cm^{-1} contained the vibrations associated with Si–O–Si. The TEOS coating has a strong, broad absorption from about 1200–1100 cm^{-1}. It has been shown that the band towards 1100 cm^{-1} corresponds to the transverse optical component of the asymmetric stretching of Si–O–Si, and at 1200 cm^{-1}, the longitudinal optical component of the same vibration [31]. The MTES coating contained a strong absorption at 1000 cm^{-1} that corresponded to the Si–O–Si asymmetric stretch [28]. The IBTES coating has a strong absorption at 1057 cm^{-1} that corresponds to the Si–O–Si asymmetric stretch [27]. The TEOS

coating has an absorption at 950 cm^{-1} due to Si–OH bending that remains in the coating due to the lower reactivity [26]. The TEOS coating also contained a small absorption at 790 cm^{-1} that corresponded to Si–O–Si bending [29]. The MTES and IBTES coating systems have strong absorptions at 760 and 740 cm^{-1}, respectively, which can be attributed to Si–C vibrations [27]. Weak absorptions at around 560 cm^{-1} corresponded to $Si–O^{-}$ rocking vibrations [29].

3.2. Effect of Modifying pH, Ageing and Thickness on Coating Failure

The material incompatibility of inorganic sol-gel coatings with organic substrates has been reported in the literature, resulting in defects such as cracking and delamination [8]. The microstructure of the TEOS coatings on polyurethane is depicted in Figure 3.

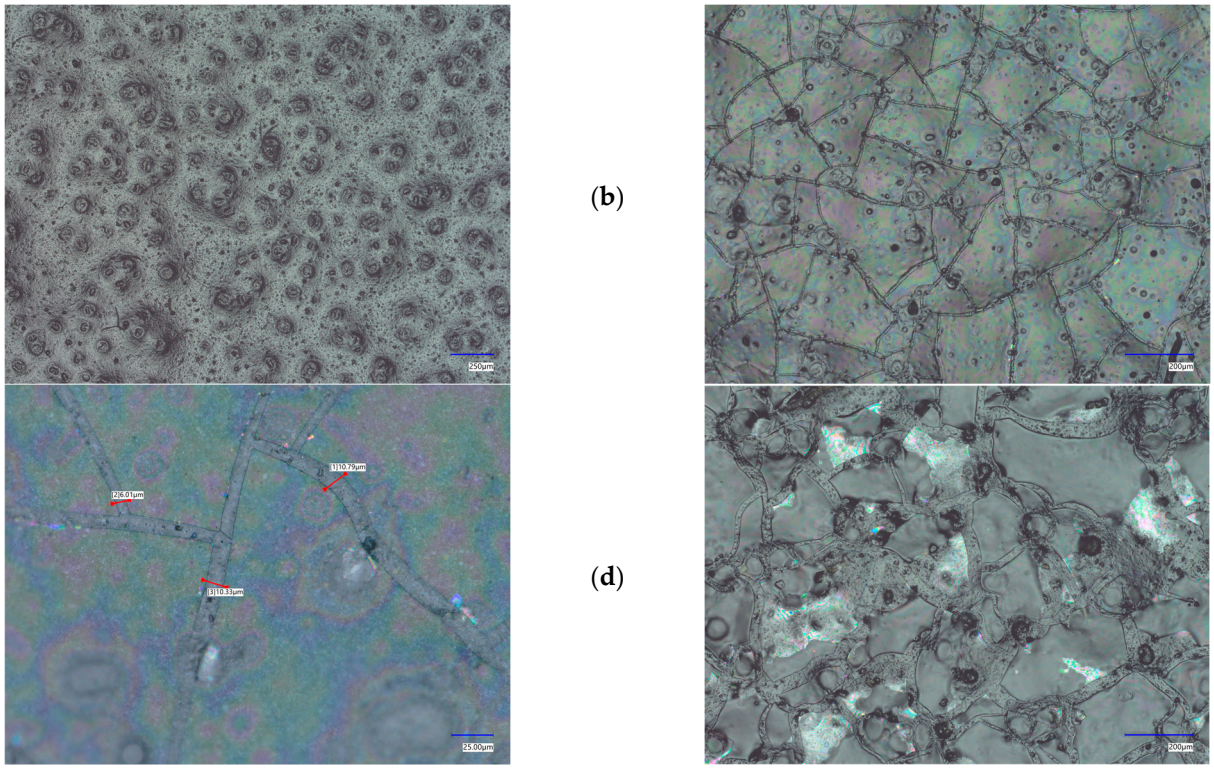

Figure 3. Micrographs: (**a**) polyurethane substrate, (**b**) TEOS coating with cracks, (**c**) measurements of crack diameters of TEOS coating and (**d**) partial delamination defects in TEOS coating.

The polyurethane substrate contains several voids on the surface that are visible in the TEOS micrograph due to the transparency of the coating. All of the TEOS coatings had cracking throughout the structure, regardless of the processing parameters. The cracks that formed ranged in diameter from 6–11 µm, as depicted in Figure 3c. This is due to the coatings exceeding the critical cracking thickness, resulting in high stresses that build within the coating and cause cracks to form [14]. Additionally, several coatings produced using TEOS had partial delamination, as depicted in Figure 3d. Partial delamination results in an exposed substrate and an undesirable sparkling effect as light diffracts differently from the substrate compared to the TEOS coating. Partial delamination of sol-gel coatings has been well reported in the literature and is often suggested to be due to high film thickness, which results in excessive stress causing partial delamination and/or poor adhesion at the interface between the substrate and the sol-gel coating [32–34]. The mechanism of adhesion for sol-gel coating systems is through the condensation of Si–OH with –OH species on the substrate surface [8]. This makes sol-gel coatings ideal for oxide-rich substrates such as metals, but polymer substrates are often limited in oxide species in comparison. Research into surface activation of polymer substrates for sol-gel coating applications has been carried

out, such as oxygen plasma activation and wet chemical etching treatments, to improve the compatibility between these two materials [8,35,36]. However, these techniques limit the industrial scalability of the sol-gel coating systems. Therefore, to understand the effects of processing parameters on coating failure (partial delamination) on the polyurethane substrate, the effects of pH, ageing and thickness were investigated. Table 3 depicts whether delamination of the TEOS-based coating occurred as a function of pH, ageing and thickness (withdrawal speed).

Table 3. Observed coating delamination as a function of pH, thickness and days of ageing. (X = delamination and ✓= no delamination).

pH	Withdrawal Speed (mm/min)	0	1	2	3	7	14	21	28
0	100	X	X	X	X	X	X	X	X
	200	X	X	X	X	X	X	X	X
2	100	X	X	X	X	X	X	X	X
	200	X	X	X	X	X	X	X	X
3	100	✓	✓	✓	✓	✓	X	X	X
	200	X	✓	✓	✓	✓	X	X	X
4	100	✓	✓	✓	✓	✓	✓	✓	✓
	200	✓	✓	✓	✓	✓	✓	✓	✓
5	100	✓	✓	✓	✓	✓	X	X	X
	200	✓	✓	✓	✓	✓	X	X	X

Analysing coating failure as a function of the processing parameters in Table 3, we can see that the sol pH plays a critical role in coating delamination. At highly acidic conditions of pH 0/2, delamination was seen in all the coatings regardless of thickness or ageing duration. Once the pH was raised to between 3–5, coatings could be produced with no delamination defects, with pH 4 coatings not delaminating after a month of ageing. The role of pH on the hydrolysis and condensation reaction rates has been well documented [37,38]. At highly acidic conditions, the hydrolysis and condensation reaction rates are fast and as the pH is increased towards neutral, the hydrolysis and condensation reaction rates slow down [37,38].

All of the coatings had cracking regardless of processing parameters, indicating the coatings were thicker than the critical cracking thickness [14]. However, as the coating stress increases further, partial delamination of the glass coating can occur. This is likely to be the case when coating organic substrates due to a material mismatch at the interface, which results in worse adhesion and higher stress within the coating [8]. In order to reduce the stress, it is beneficial to have hydroxyl groups within the coating and on the substrate available for interfacial bonding [8]. Therefore, it is possible that in very acidic conditions, where the condensation reaction rates are much higher, a lower amount of hydroxyl groups are present at the interface, resulting in higher stresses and causing delamination to occur. In order to investigate this theory, the Si–O–Si/Si–OH band intensity ratio on the FTIR was measured as a function of solution pH, which provides a measure for the development of the coating [39]. A higher ratio would indicate strong Si–O–Si development and/or low Si–OH remaining within the coating network. The results are depicted in Figure 4.

The Si–O–Si/Si–OH ratio for a highly acidic pH of 0/2 is much higher than pH 3–5. This suggests strong development of the polysiloxane network due to the strong Si–O–Si signal but also a reduced number of Si–OH in the final coating. This combination likely results in higher strains within the coating compared to the pH 3–5 coating systems, which causes partial delamination to occur.

To further test this theory, the polyurethane substrate underwent oxygen plasma activation, which resulted in a reduction of the WCA from 73° to 24°, as hydrophilic hydroxyl groups formed on the surface of the polymeric substrate. The TEOS coating was then deposited at a pH of 0, which resulted in no partial delamination. This suggests the presence of hydroxyl species at the interface between the substrate and the coating plays a

critical role in the final stress of the coating system and the potential for defects such as delamination. The processing parameters pH 4 and one day of ageing were chosen for the rest of this study due to the long-term stability against delamination and suitability for scale-up operations.

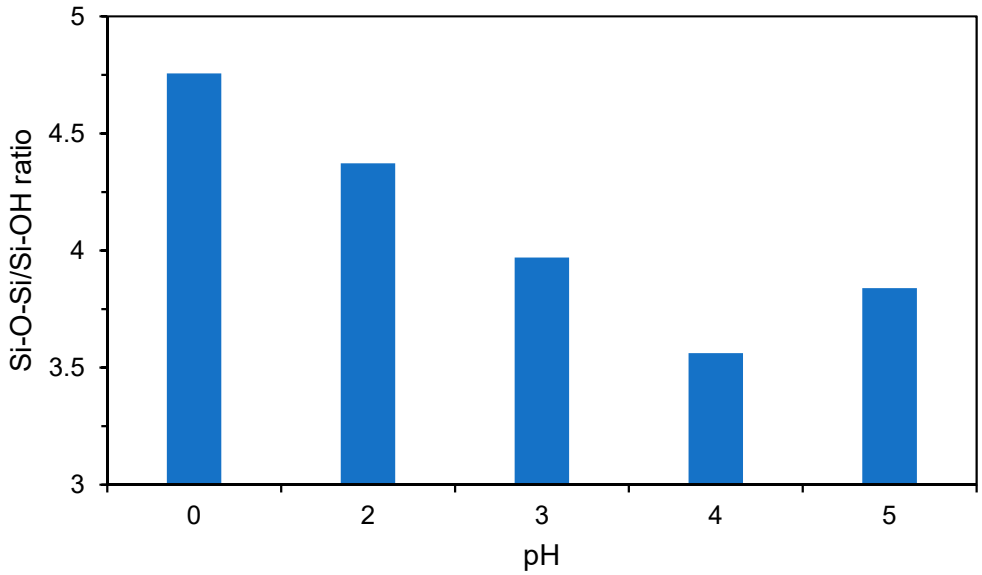

Figure 4. FTIR Si–O–Si/Si–OH ratio of cured coatings as a function of pH.

3.3. Coating Deposition, Surface Analysis and Mechanical Properties

It is of industrial interest to utilise deposition technologies that can be scaled up to high line speeds in the order of 10–100 m/s. Therefore, spray and bar coating of the sol-gel coatings were investigated. The resultant microstructures of the bar and spray coatings for the precursors TEOS, MTES and IBTES are depicted in Figure 5.

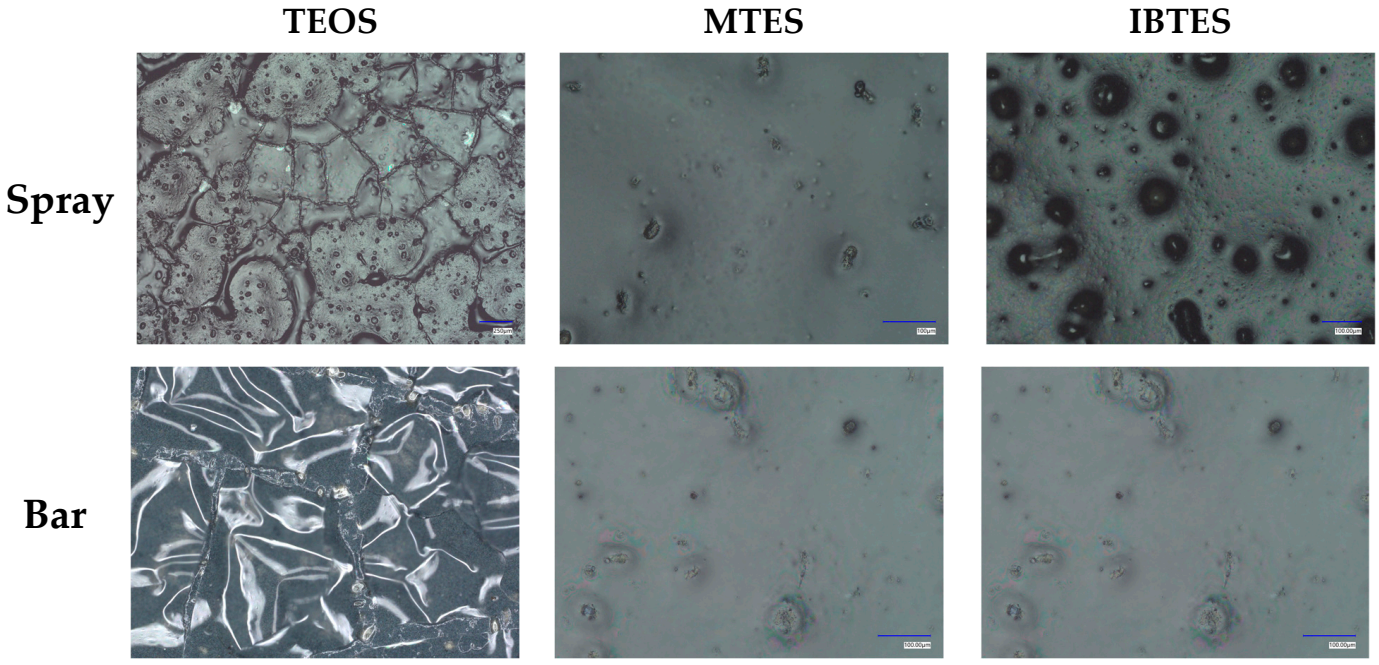

Figure 5. Micrographs of the bar and spray-coated TEOS, MTES and IBTES on a polyurethane substrate.

Visual observations, shown in Figure 5, of coating TEOS onto the polyurethane surface via spray or bar coating methods showed that the TEOS coating was unable to wet the surface and form a homogeneous layer. This could be due to the limited thickness of the TEOS-based coatings before excess stress results in delamination and limits applicability for high-speed applications such as the coil-coating line. The IBTES and MTES coatings formed a homogenous defect-free layer using spray and bar coating techniques. This is due to the much more flexible nature of the coatings through the incorporation of organic alkyl chains within the coating, which allows thicker coatings to be produced [18]. The hybrid coatings did not have cracks due to lower coating stresses, unlike the TEOS-based coatings [14]. However, the spray-coated IBTES had poor wetting on the substrate, resulting in craters forming, as depicted in Figure 5. The coatings utilised in this study, and the resultant topographical properties are depicted in Table 4.

Table 4. Topographical measurements of coatings.

Sample	R_a Roughness (μm)	Contact Angle (°)	Film Thickness (μm)
Polyurethane	0.41 ± 0.02	73.4 ± 0.84	15 ± 1
Polyurethane Clearcoat	0.46 ± 0.01	74.6 ± 0.33	20 ± 1
TEOS Dip	0.52 ± 0.03	79.3 ± 0.56	0.87 ± 0.10
MTES Bar	0.32 ± 0.01	93.1 ± 0.43	2.35 ± 0.07
MTES Spray	0.38 ± 0.02	91.2 ± 1.29	2.62 ± 0.16
IBTES Bar	0.54 ± 0.04	95.9 ± 1.76	2.96 ± 0.35
IBTES Spray	0.81 ± 0.07	92.7 ± 2.02	3.45 ± 0.42

The MTES coating results in a smoother surface compared to the polyurethane, TEOS and IBTES coatings. The IBTES coating is considerably rougher than the other coatings. This may be due to the bulky isobutyl groups, which limit network formation and cause higher surface roughness. The WCA of MTES and IBTES is higher than that of TEOS and polyurethane coating systems because of the alkyl chains that align at the surface and repel water [40]. The film thickness of the sol-gel coating systems is an order of magnitude lower than the organic coatings typically used. The hybrid coatings are much thicker than the TEOS coating due to the coating deposition techniques used and the increased flexibility that allows the thicker coatings to be produced.

The mechanical properties typically assessed for organically coated steel substrates were evaluated for the novel coating systems and are depicted in Table 5.

Table 5. Qualitative mechanical properties of the coating systems.

Sample	Pencil Hardness	T-Bend	Adhesion
Polyurethane	H	0T	5B
TEOS Dip	3H	0T	5B
MTES Bar	2H	0T	5B
MTES Spray	2H	0T	5B
IBTES Bar	H	0T	5B
IBTES Spray	H	0T	5B

The pencil hardness test is a fast method to evaluate the hardness of coatings using pencils of hardness from 6B to 6H, whereby 6B is the softest, and 6H is the hardest. The test consists of making scratches on the coating with a pencil at a 45° angle against the substrate. The pencil hardness is the softest pencil that forms a scratch. The TEOS and MTES coatings displayed an increased pencil hardness when compared to the uncoated polyurethane. However, the IBTES coatings had no change in pencil hardness compared to the uncoated polyurethane. The TEOS-based coatings have the highest hardness as they are completely inorganic, whereas, for the MTES and IBTES coatings, there is an organic component that reduces the hardness of the coating, which has been suggested

to be due to reduced crosslinking compared to the TEOS system [41]. This effect is more substantial for the IBTES coatings that contain a higher proportion of organic chains. An important characteristic of coil coatings is coating formability. The coatings are deposited and cured before forming the steel. Therefore, the coatings must have resistance to failure by cracking and delamination during forming to maintain the protection of the steel [42]. The T-bend test is used to assess coating formability and adhesion. The highest rating, '0T', corresponds to a 180° bend of the steel, resulting in the highest potential surface strain [42]. All the coatings had a T-bend rating of '0T', indicating excellent formability and adhesion. Finally, the adhesion of the coatings was assessed using the cross-hatch adhesion test. All the coating systems had the top result of '5B', indicating that during the test, none of the coatings delaminated at all. This demonstrates that the coatings had excellent adhesion to the polyurethane substrate, which is important for long-term durability.

3.4. Effect of Curing

The curing temperature and duration have a significant effect on the properties of sol-gel coatings [43]. Curing conditions will affect the rate and extent of crosslinking that occurs in sol-gel coatings. Higher temperatures and longer curing durations are associated with a greater overall cure of the sol-gel coating. Organically coated steels are typically cured at a PMT of 232 °C for 45 s and are, therefore, limited in the temperature they can be subjected to before thermal degradation initiates. In addition, it is beneficial to minimise curing duration and temperature to improve industrial scalability and reduce costs and the carbon footprint of the coatings. The processing conditions required to produce a stable and homogeneous sol-gel coating applied to a polyurethane substrate must be understood to determine the feasibility of industrial applications.

3.4.1. FTIR Analysis

The effect of curing times and temperatures on the sol-gel coatings was investigated using FTIR, surface roughness and contact angle measurements. The effect of increased curing temperature on the structure of the sol-gel coatings results in a decrease in the Si-OH in the coatings as the condensation reactions accelerate, resulting in increased densification and Si–O–Si formation [39]. This is depicted in Figure 6b for the MTES coatings cured for 12 min.

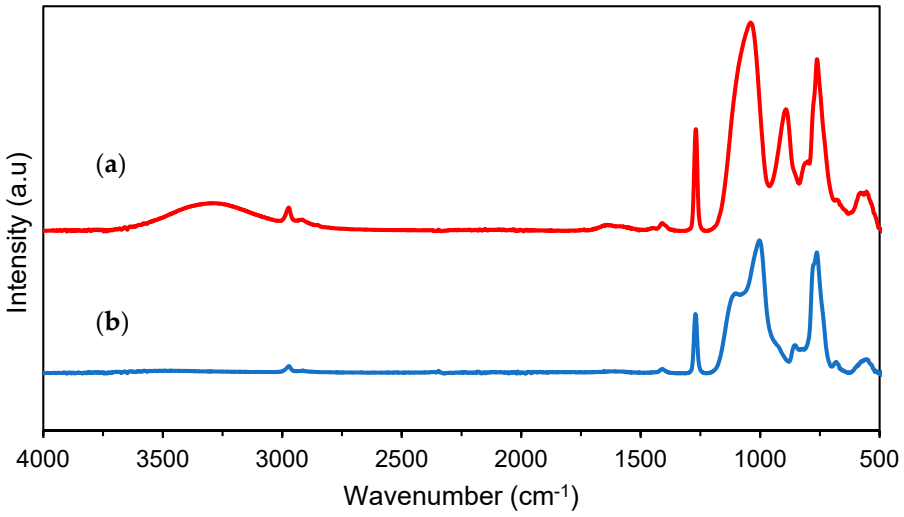

Figure 6. FTIR spectra of MTES coating: (**a**) RT cure and (**b**) 210 °C PMT for 12 min.

As the curing temperatures increase, the Si–OH stretch at about 3200–3400 cm^{-1} becomes significantly weaker. A quantitative analysis of the FTIR bands was carried out using the ratio between the band intensity for the Si–OH peak at 3200–3400 cm^{-1} and the Si–O–Si peak at 1100 cm^{-1}. The evolution of the Si–O–Si/Si–OH band intensity ratio as a function of curing temperature and time for the TEOS coatings at withdrawal speeds of 100 and 200 mm/min is depicted in Figure 7.

It can be seen in Figure 7a that regardless of curing duration and temperature, the withdrawal speed had a small effect on the curing of the coating systems. However, the curing duration had a large effect on the Si–O–Si/Si–OH ratio. This is expected as the coatings have more time to undergo condensation reactions, resulting in a denser network. The role of temperature may be more critical than curing duration; curing the coatings at a PMT of 232 °C for 45 s resulted in an equivalent Si–O–Si/Si–OH ratio as a 12 min cure at a PMT of 175 °C. Therefore, the curing conditions of 232 °C for 45 s were optimal for ensuring network development of the glass coatings without affecting the polymeric substrate while improving the industrial scalability to the coil-coating lines.

The Si–O–Si/Si–OH ratios for the MTES and IBTES coatings were significantly larger than the TEOS-based coatings. This indicates a denser coating network has formed, which was expected due to the increased reactivity of hybrid precursors in acidic conditions due to the inductive effect of the organic chains [18]. The IBTES coatings had a decrease in Si–O–Si/Si–OH ratios at high curing temperatures and curing durations. This is likely due to the degradation of the isobutyl groups, which causes a decrease in the Si–O–Si/Si–OH ratio [44]. The results in Figure 7 show that there is a clear benefit to using the OIH coatings MTES and IBTES, as they can be cured at lower temperatures and for shorter durations compared to the inorganic TEOS coatings.

3.4.2. Surface Properties

The effect of curing temperature and duration on the surface properties of roughness and water contact angle (WCA) of the coating systems was evaluated and is depicted in Figure 8.

As depicted in Figure 8a the withdrawal speed of the TEOS coatings affects the surface roughness at all temperatures and curing durations. This could be because the higher withdrawal speeds result in thicker coatings that shrink more during curing, which results in a rougher surface [45]. For all coating systems, as the curing temperature increases, the surface becomes rougher as the coating systems become denser. The IBTES coatings were noticeably rougher than the MTES coatings, which may be due to worse network formation due to the bulky isobutyl groups.

The WCA for all the coating systems increases as a function of curing temperature and duration. This is because as the curing reaction occurs, hydrophilic Si–OH groups are converted to less hydrophilic Si–O–Si groups, which causes an increase in the WCA [40]. The hybrid coatings MTES and IBTES reach their peak WCA faster than the TEOS coatings as the alkyl chains align at the surface. In addition, hybrid coatings have a higher WCA due to their hydrophobic alkyl chains [40].

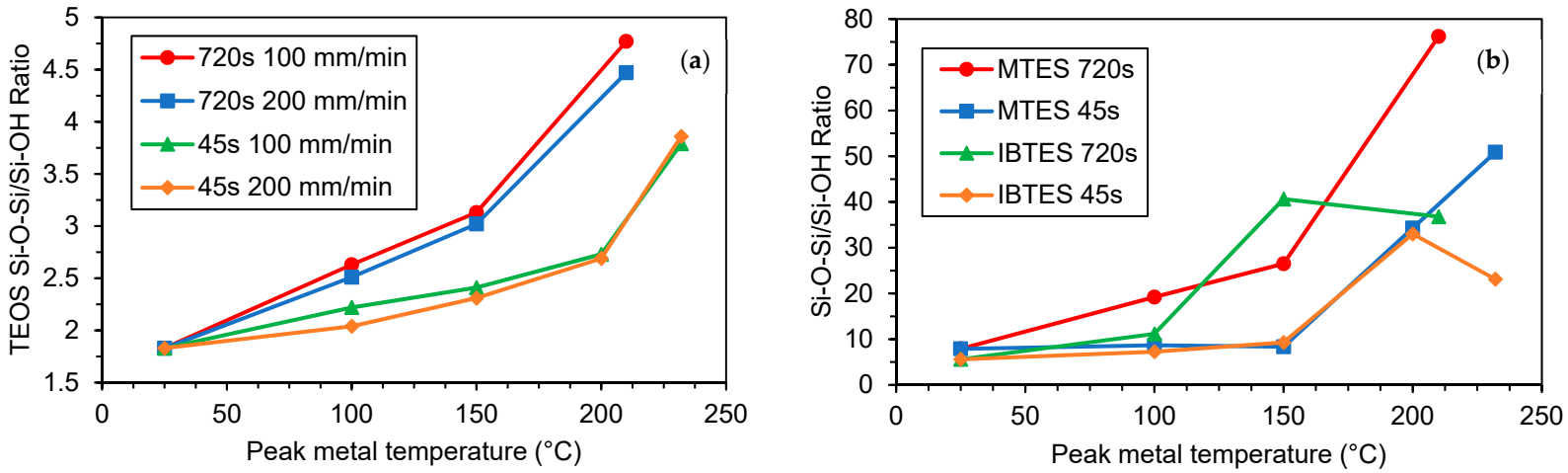

Figure 7. Si–O–Si/Si–OH ratio as a function of temperature and duration for (**a**) TEOS at different dip-coating withdrawal speeds and (**b**) MTES and IBTES.

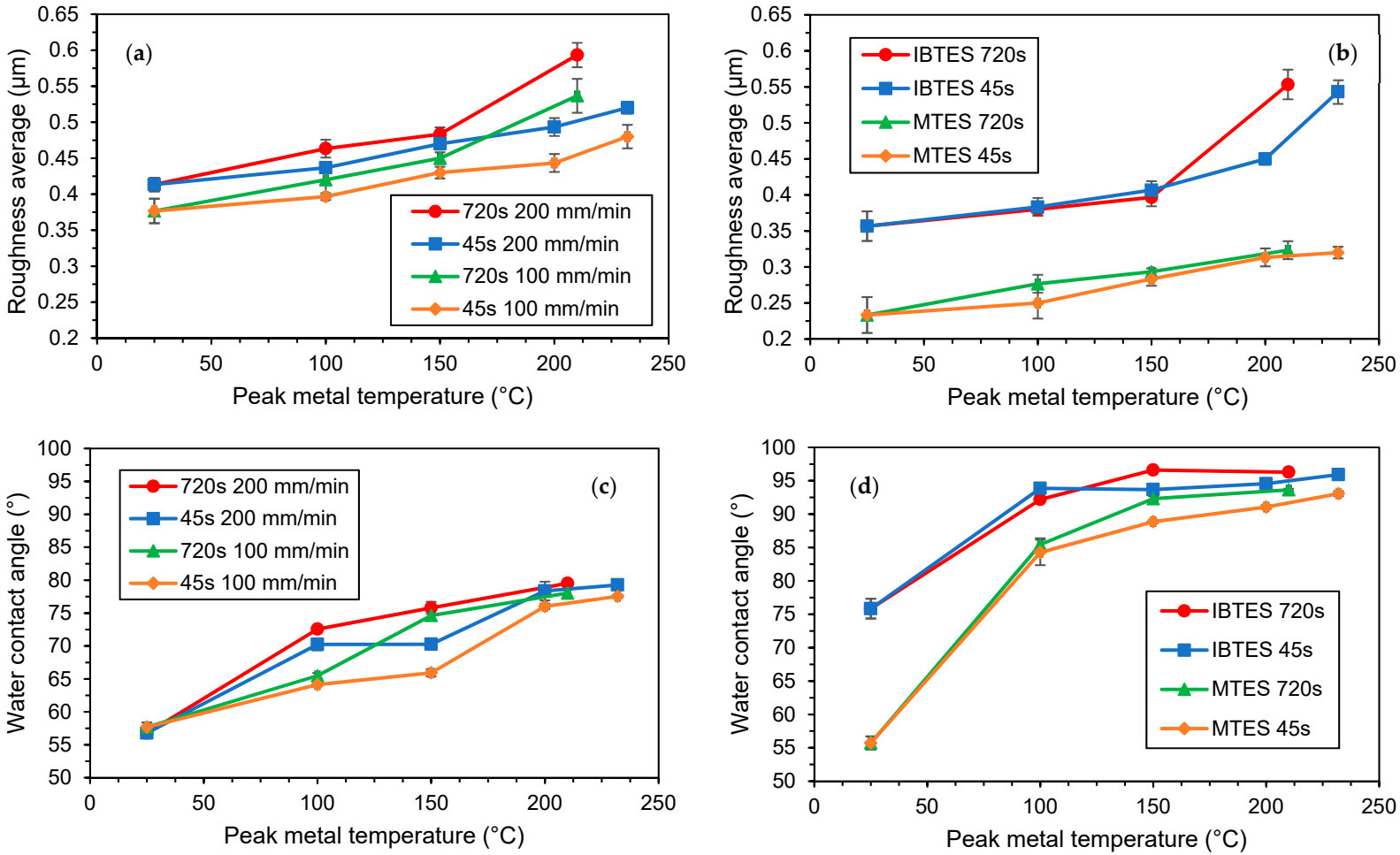

Figure 8. Ra and WCA as a function of temperature and curing duration for (**a**,**c**) TEOS at different dip-coating withdrawal speeds and (**b**,**d**) MTES and IBTES.

3.5. Accelerated Laboratory Weathering

The polyurethane and sol-gel coatings were subjected to accelerated weathering cycles of condensation and UV radiation, designed to emulate exposure to humidity, precipitation, and to sunlight. This allowed for an accelerated evaluation of the degradation and durability of the sol-gel coating systems to determine their suitability as outdoor clearcoat materials [46]. The IBTES-coated polyurethane samples produced via the spraying technique were observed to rapidly fail when subjected to accelerated weathering and were, therefore, discounted from further analysis. The FTIR spectra before and after accelerated weathering for each coating system are shown in Figure 9.

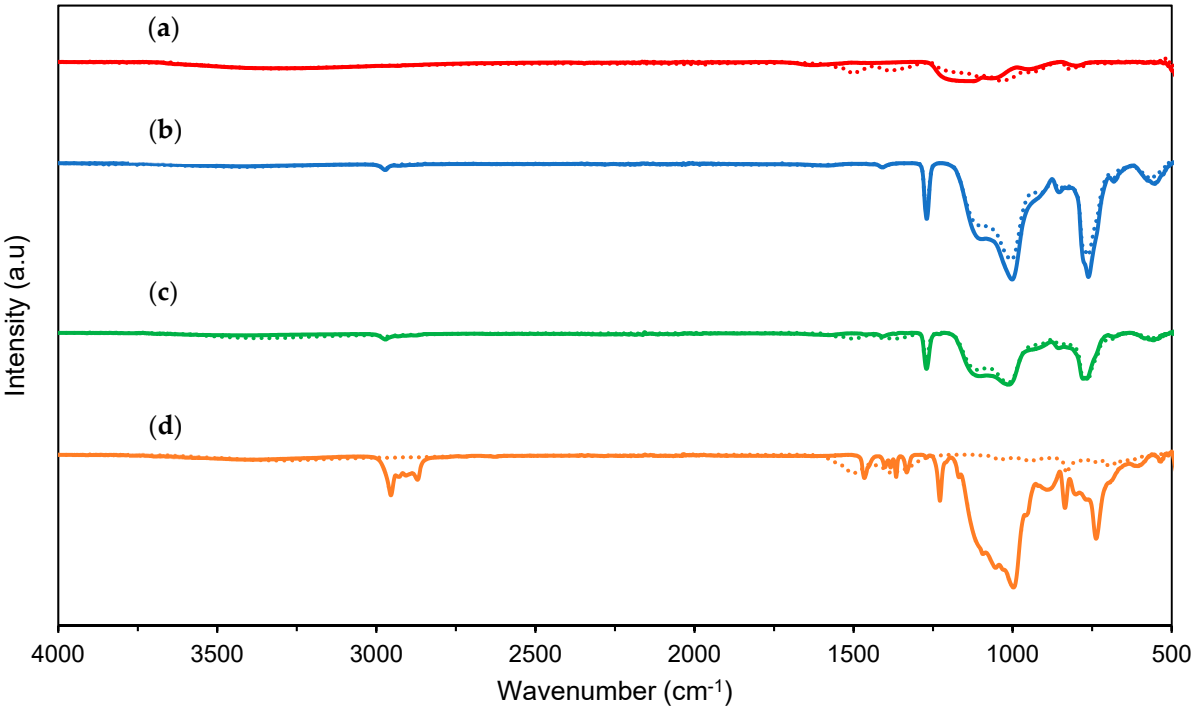

Figure 9. FTIR spectra before (–) and after (. . . 4000 h of accelerated weathering for the coatings (**a**) TEOS, (**b**) MTES Spray, (**c**) MTES Bar and (**d**) IBTES Bar.

Silica is known to degrade when in contact with water through hydrolysis of the polysiloxane network [47]. The hydrolytic degradation of solid silica is depicted below.

$$SiO_{2_{(s)}} + 2H_2O \leftrightarrow Si(OH)_{4\ (aq)} \quad (3)$$

Diaz et al. studied the degradation of combined TEOS:MTES coatings when exposed to water and found that the greater the TEOS content, the faster the coatings degraded [19]. They proposed that the rate of degradation correlated with hydrophilicity; the more hydrophobic MTES coatings functioned as a better barrier to water entering the coating network, while the TEOS coatings had greater water flow through the coating network [19].

Comparing the FTIR spectra before and after accelerated weathering, the appearance of two new weak peaks at 1500 and 1370 cm^{-1} after weathering corresponds to HDG corrosion products such as $ZnCO_3$ [48,49]. At high humidity and under UV light, the coatings MTES and TEOS were demonstrated to be durable and resistant to this type of environment. The TEOS coating has undergone some degradation, with a reduction in the intensity of the shoulder of the Si–O–Si peak at 1200 cm^{-1}, while the MTES coating systems remained largely unchanged. This could be attributed to the hydrophobicity of the MTES coating system. However, the IBTES coating system, which is also hydrophobic, degraded the fastest out of the coating systems tested and is not suitable for this type of environment. The FTIR spectrum of IBTES after weathering demonstrated the coating

is largely not present anymore due to rapid degradation. It is, therefore, possible that although the IBTES coating is hydrophobic as well, the isobutyl alkyl chain renders the coating susceptible to photodegradation, and/or water is passing through the coating system due to pores within the IBTES coating. Coatings with a higher porosity and surface area result in increased contact with water, potentially accelerating hydrolytic degradation of the coating [19]. It is likely that the IBTES coating structure is more porous than the TEOS and MTES coatings due to the bulky isobutyl group throughout the coating, which could favour water flow throughout the material. Rapid loss of WCA of isobutyl coatings was reported when exposed to accelerated weathering, which was attributed to oxidative degradation, confirming our results of poor durability of the IBTES coating system [44].

The aesthetic properties of gloss retention and colour change were measured as a function of weathering. The lifetime of the coatings for coil-coated steel can be extended by using materials that are resistant to environmental degradation, resulting in a coating system that maintains properties such as gloss retention and minimal colour change due to degradation, which is utilised for product guarantees. The gloss retention (%) and colour change (ΔE) for the coating systems after 4000 h of accelerated weathering are depicted in Figure 10.

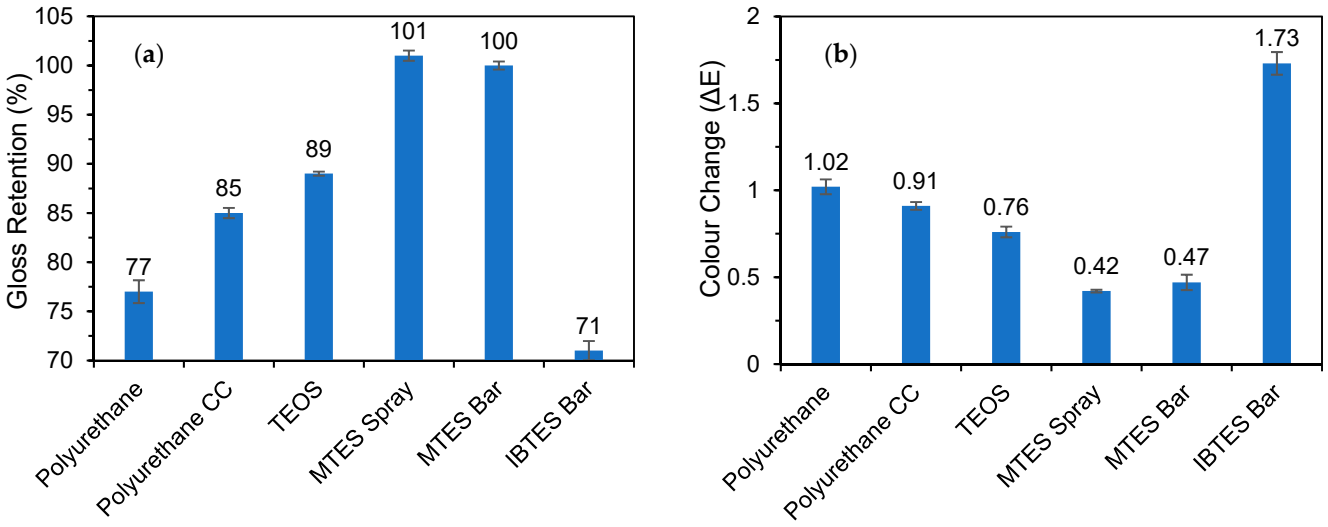

Figure 10. Aesthetic properties of coating systems after 4000 h of accelerated weathering: (**a**) gloss retention (%) and (**b**) colour change (ΔE).

The gloss retention results demonstrated the superior durability of the TEOS and MTES coating systems in retaining gloss when exposed to weathering compared to the organic polyurethane coating systems. The MTES coating systems had no gloss loss over 4000 h, retaining the same appearance as when the test was started. This is due to a lack of degradation occurring at the surface level, which results in a rougher surface and, thus, a reduction in gloss, which is seen in the polyurethane coatings. The IBTES coating system had a significant gloss loss of 29%, which indicated the IBTES coating is more susceptible to degradation by UV light and water.

The coating systems TEOS and MTES demonstrated minimal colour change. However, the IBTES coating system had a much higher colour change of 1.73. The degradation of the isobutyl chain within the IBTES coating network could cause a significant colour change to be observed [44]. For durability and aesthetics as a clearcoat material, the MTES coating systems offered excellent durability that outperformed the polyurethane substrate and polyurethane clearcoat.

The utilisation of these coating systems could allow for longer-lasting aesthetics for building systems and other potential applications, increasing the lifetime of coated products. The coating performance could be further improved through the inclusion of light stabilisers. The inclusion of the bulky isobutyl chain in the IBTES coating resulted

in a coating system that was much more susceptible to degradation and had fast gloss loss and colour change. Therefore, the IBTES coating would be less suitable as an outdoor clearcoat material.

4. Conclusions

The utilisation of glass-like clearcoats over polyurethane substrates for coil-coating applications was explored to determine their feasibility and typical properties. The sol-gel precursors TEOS, MTES and IBTES were used to alter the chemistry of the glass coating systems. TEOS-coated polyurethane substrates were observed to have cracking and delamination defects, which have been attributed to high stresses within the coating. A systematic study whereby variables such as solution pH, ageing time and coating thickness were varied to determine if a suitable, defect-free TEOS coating could be produced. Modification of the pH to between 3–5 allowed for TEOS coatings without delamination to be produced over a polyurethane substrate. However, due to the high stresses and limited thickness of the TEOS coatings, they could not be deposited using high-speed deposition techniques such as spray and bar coating. Therefore, they would not be suitable for high-speed industrial application when applied to a polyurethane substrate.

The modification of the sol-gel precursor by introducing organic components resulted in improved flexibility that allowed deposition by spray and bar coating techniques. Furthermore, the MTES and IBTES coatings demonstrated improved network development due to faster curing reactions. This proved beneficial for lower curing times and shorter duration utilised on the coil-coating line. Therefore, they may be suitable for use at scale in an industrial application.

The sol-gel coatings demonstrated excellent mechanical properties, which resulted in a harder surface, excellent adhesion and flexibility which is critical for coil-coated steel to undergo forming. Accelerated weathering QUV testing over 4000 h demonstrated superior long-term aesthetics for the MTES coatings compared to the polyurethanes tested, which could result in buildings that maintain their new appearance for much longer. FTIR analysis after accelerated weathering showed the high durability of the MTES and TEOS coating systems when exposed to weathering due to the inorganic makeup of the coating systems.

The use of sol-gel coatings for coil-coating applications could result in significant material, CO_2 and volatile organic compound reductions [15]. Additionally, the glass coatings are not produced using fossil-fuel feedstocks but are produced using abundant silica feedstock. The glass coating systems could find widespread use as a durable, high processability, low-cost and environmentally friendly alternative to fossil fuel-based coating systems for a variety of applications on organic substrates and surfaces that are high in oxide content, such as metals and ceramics.

Future work aims to evaluate the barrier properties of the glass coating systems and the utilisation of additives within the coatings to further improve performance and introduce functionalities.

Author Contributions: Conceptualisation, E.W., C.G., C.B., M.C. and P.B.; methodology, E.W., C.G., C.B. and M.C.; validation, E.W., C.G., C.B., M.C. and P.B.; formal analysis, E.W., C.G., C.B. and M.C.; investigation, E.W., C.G., C.B. and M.C.; resources, M.C. and P.B.; data curation, E.W.; writing—original draft preparation, E.W.; writing—review and editing, E.W., C.G., C.B. and M.C.; visualisation, E.W.; supervision, M.C. and P.B.; project administration, M.C. and P.B.; funding acquisition, M.C. and P.B. All authors have read and agreed to the published version of the manuscript.

Funding: The authors would like to acknowledge the COATED M2A funding from the European Social Fund via the Welsh Government (c80816), the Engineering and Physical Sciences Research Council (Grant Ref: EP/S02252X/1) and Tata Steel UK that has made this research possible.

Institutional Review Board Statement: Not applicable.

Informed Consent Statement: Not applicable.

Data Availability Statement: The data used to support the findings of this study are included within the article and are available from the corresponding author upon request.

Conflicts of Interest: The authors declare no conflict of interest.

References

1. Engels, H.-W.; Pirkl, H.-G.; Albers, R.; Albach, R.W.; Krause, J.; Hoffmann, A.; Casselmann, H.; Dormish, J. Polyurethanes: Versatile Materials and Sustainable Problem Solvers for Today's Challenges. *Angew. Chem. Int. Ed.* **2013**, *52*, 9422–9441. [CrossRef]
2. Miklečić, J.; Turkulin, H.; Jirouš-Rajković, V. Weathering Performance of Surface of Thermally Modified Wood Finished with Nanoparticles-Modified Waterborne Polyacrylate Coatings. *Appl. Surf. Sci.* **2017**, *408*, 103–109. [CrossRef]
3. Siyab, N.; Tenbusch, S.; Willis, S.; Lowe, C.; Maxted, J. Going Green: Making Reality Match Ambition for Sustainable Coil Coatings. *J. Coat. Technol. Res.* **2016**, *13*, 629–643. [CrossRef]
4. Figueira, R.B.; Fontinha, I.R.; Silva, C.J.R.; Pereira, E.V. Hybrid Sol-Gel Coatings: Smart and Green Materials for Corrosion Mitigation. *Coatings* **2016**, *6*, 12. [CrossRef]
5. Figueira, R.B.; Silva, C.J.R.; Pereira, E.V. Influence of Experimental Parameters Using the Dip-Coating Method on the Barrier Performance of Hybrid Sol-Gel Coatings in Strong Alkaline Environments. *Coatings* **2015**, *5*, 124–141. [CrossRef]
6. Wint, N.; Wijesinghe, S.L.; Yan, W.; Ong, W.K.; Wu, L.Y.; Williams, G.; Mcmurray, H.N. The Sacrificial Protection of Steel by Zinc-Containing Sol-Gel Coatings. *J. Electrochem. Soc.* **2019**, *166*, C434–C444. [CrossRef]
7. Hernández-Del Castillo, P.C.; Oliva, J.; Robledo-Trujillo, G.; Rodríguez-González, V. Enhancing the Eosin-Yellowish Dye Degradation in Drinking Water by Using TiO_2 Coatings Co-Doped with Ni and In. *Environ. Sci. Pollut. Res.* **2023**, *30*, 5258–5266. [CrossRef]
8. Chou, T.P.; Cao, G. Adhesion of Sol-Gel-Derived Organic-Inorganic Hybrid Coatings on Polyester. *J. Solgel Sci. Technol.* **2003**, *27*, 31–41. [CrossRef]
9. Wu, L.Y.L.; Boon, L.; Chen, Z.; Zeng, X.T. Adhesion Enhancement of Sol–Gel Coating on Polycarbonate by Heated Impregnation Treatment. *Thin Solid Films* **2009**, *517*, 4850–4856. [CrossRef]
10. Wang, D.; Bierwagen, G.P. Sol–Gel Coatings on Metals for Corrosion Protection. *Prog. Org. Coat.* **2009**, *64*, 327–338. [CrossRef]
11. Figueira, R.B. Hybrid Sol–Gel Coatings for Corrosion Mitigation: A Critical Review. *Polymers* **2020**, *12*, 689. [CrossRef] [PubMed]
12. Barroso, G.; Li, Q.; Bordia, R.K.; Motz, G. Polymeric and Ceramic Silicon-Based Coatings—A Review. *J. Mater. Chem. A* **2019**, *7*, 1936–1963. [CrossRef]
13. Vidal, K.; Gómez, E.; Goitandia, A.M.; Angulo-Ibáñez, A.; Aranzabe, E. The Synthesis of a Superhydrophobic and Thermal Stable Silica Coating via Sol-Gel Process. *Coatings* **2019**, *9*, 627. [CrossRef]
14. Kozuka, H. Stress Evolution and Cracking in Sol-Gel-Derived Thin Films. In *Handbook of Sol-Gel Science and Technology*; Springer International Publishing: Cham, Switzerland, 2018; pp. 275–311.
15. Ciriminna, R.; Pagliaro, M.; Palmisano, G. Sol-Gel for Environmentally Green Products. In *The Sol-Gel Handbook*; Wiley-VCH Verlag GmbH & Co. KGaA: Weinheim, Germany, 2015; pp. 1055–1070.
16. Ciriminna, R.; Scurria, A.; Pagliaro, M. Sustainability Evaluation of AquaSun Antifouling Coating Production. *Coatings* **2022**, *12*, 1034. [CrossRef]
17. Igal, K.; Zanotti, K.; Zuin, V.G.; Vazquez, P. Sol-Gel Technology for Greener and More Sustainable Antimicrobial Textiles That Use Silica Matrices with C, and Ag and ZnO as Biocides. *Curr. Res. Green. Sustain. Chem.* **2021**, *4*, 100177. [CrossRef]
18. Schubert, U. Chemistry and Fundamentals of the Sol-Gel Process. In *The Sol-Gel Handbook*; Wiley-VCH Verlag GmbH & Co. KGaA: Weinheim, Germany, 2015; pp. 1–28.
19. Juan-Díaz, M.J.; Martínez-Ibáñez, M.; Hernández-Escolano, M.; Cabedo, L.; Izquierdo, R.; Suay, J.; Gurruchaga, M.; Goñi, I. Study of the Degradation of Hybrid Sol–Gel Coatings in Aqueous Medium. *Prog. Org. Coat.* **2014**, *77*, 1799–1806. [CrossRef]
20. *BS EN 13523-3*; Coil Coated Metals—Test Methods—Colour Difference. BSI (British Standards Institute): London, UK, 2014.
21. *BS EN 13523-2*; Coil Coated Metals. Test Methods—Gloss. BSI (British Standard Institute): London, UK, 2014.
22. *BS EN 13523-4*; Standard Coil Coated Metals. Test Methods—Pencil Hardness. BSI (British Standards Institute): London, UK, 2014.
23. *BS EN 13523-6*; Coil Coated Metals. Test Methods—Adhesion after Indentation (Cupping Test). BSI (British Standards Institute): London, UK, 2020.
24. *BS EN 13523-7*; Coil Coated Metals. Test Methods—Resistance to Cracking on Bending (T-Bend Test). BSI (British Standards Institute): London, UK, 2021.
25. *BS EN 13523-10*; Coil Coated Metals. Test Methods—Resistance to Fluorescent UV Radiation and Water Condensation. BSI (British Standards Institute): London, UK, 2017.
26. Post, P.; Wurlitzer, L.; Maus-Friedrichs, W.; Weber, A.P. Characterization and Applications of Nanoparticles Modified In-Flight with Silica or Silica-Organic Coatings. *Nanomaterials* **2018**, *8*, 530. [CrossRef] [PubMed]
27. Al-Oweini, R.; El-Rassy, H. Synthesis and Characterization by FTIR Spectroscopy of Silica Aerogels Prepared Using Several $Si(OR)_4$ and $R''Si(OR')_3$ Precursors. *J. Mol. Struct.* **2009**, *919*, 140–145. [CrossRef]
28. Almeida, R.M.; Marques, A.C. Characterization of Sol–Gel Materials by Infrared Spectroscopy. In *Handbook of Sol-Gel Science and Technology*; Springer International Publishing: Cham, Switzerland, 2016; pp. 1–31.

29. Capeletti, L.B.; Zimnoch, J.H. Fourier Transform Infrared and Raman Characterization of Silica-Based Materials. In *Applications of Molecular Spectroscopy to Current Research in the Chemical and Biological Sciences*; InTech: London, UK, 2016.
30. Gunzler, H.; Gremlich, H. *IR Spectroscopy: An Introduction*; Wiley-VCH: Weinheim, Germany, 2002; Volume 69469.
31. Almeida, R.M.; Pantano, C.G. Structural Investigation of Silica Gel Films by Infrared Spectroscopy. *J. Appl. Phys.* **1990**, *68*, 4225–4232. [CrossRef]
32. Chan, C.M.; Cao, G.Z.; Fong, H.; Sarikaya, M.; Robinson, T.; Nelson, L. Nanoindentation and Adhesion of Sol-Gel-Derived Hard Coatings on Polyester. *J. Mater. Res.* **2000**, *15*, 148–154. [CrossRef]
33. Jeffrey Brinker, C.; Hurd, A.J. Fundamentals of Sol-Gel Dip-Coating. *J. Phys. III* **1994**, *4*, 1231–1242. [CrossRef]
34. Marthelot, J.; Bico, J.; Melo, F.; Roman, B. A New Failure Mechanism in Thin Film by Collaborative Fracture and Delamination: Interacting Duos of Cracks. *J. Mech. Phys. Solids* **2015**, *84*, 214–229. [CrossRef]
35. Gururaj, T.; Subasri, R.; Raju, K.R.C.S.; Padmanabham, G. Effect of Plasma Pretreatment on Adhesion and Mechanical Properties of UV-Curable Coatings on Plastics. *Appl. Surf. Sci.* **2011**, *257*, 4360–4364. [CrossRef]
36. Raju, K.R.C.S.; Sowntharya, L.; Lavanya, S.; Subasri, R. Effect of Plasma Pretreatment on Adhesion and Mechanical Properties of Sol-Gel Nanocomposite Coatings on Polycarbonate. *Compos. Interfaces* **2012**, *19*, 259–270. [CrossRef]
37. Brinker, C.J.; Scherer, G.W. *The Physics and Chemistry of Sol-Gel Processing*; Elsevier: Amsterdam, Netherlands, 1990; ISBN 9780080571034.
38. Innocenzi, P. From the Precursor to a Sol. In *The Sol to Gel Transition*; Springer: New York, NY, USA, 2016; pp. 7–25.
39. Fedel, M.; Poelman, M.; Zago, M.; Vandermiers, C.; Cossement, D.; Olivier, M.-G.; Deflorian, F. Influence of Formulation and Application Parameters on the Performances of a Sol–Gel/Clay Nanocomposite on the Corrosion Resistance of Hot-Dip Galvanized Steel. Part II. Effect of Curing Temperature and Time. *Surf. Coat. Technol.* **2015**, *274*, 9–17. [CrossRef]
40. Basu, B.J.; Hariprakash, V.; Aruna, S.T.; Lakshmi, R.V.; Manasa, J.; Shruthi, B.S. Effect of Microstructure and Surface Roughness on the Wettability of Superhydrophobic Sol–Gel Nanocomposite Coatings. *J. Sol-Gel Sci. Technol.* **2010**, *56*, 278–286. [CrossRef]
41. Le Bail, N.; Benayoun, S.; Toury, B. Mechanical Properties of Sol–Gel Coatings on Polycarbonate: A Review. *J. Solgel Sci. Technol.* **2015**, *75*, 710–719. [CrossRef]
42. Sorce, F.S.; Ngo, S.; Lowe, C.; Taylor, A.C. Quantification and Analysis of Coating Surface Strains in T-Bend Tests. *Int. J. Adv. Manuf. Technol.* **2021**, *113*, 1125–1142. [CrossRef]
43. Rafiaei, F.; Naderi, R.; Dehghanian, C. Impact of Curing on the Corrosion Performance of an Eco-Friendly Silane Sol–Gel Coating on 304L Stainless Steel. *RSC Adv.* **2015**, *5*, 43225–43233. [CrossRef]
44. Xiu, Y.; Hess, D.W.; Wong, C.P. UV and Thermally Stable Superhydrophobic Coatings from Sol–Gel Processing. *J. Colloid. Interface Sci.* **2008**, *326*, 465–470. [CrossRef]
45. Rosero-Navarro, N.C.; Figiel, P.; Jedrzejewski, R.; Biedunkiewicz, A.; Castro, Y.; Aparicio, M.; Pellice, S.A.; Durán, A. Influence of Cerium Concentration on the Structure and Properties of Silica-Methacrylate Sol–Gel Coatings. *J. Sol-Gel Sci. Technol.* **2010**, *54*, 301–311. [CrossRef]
46. Wypych, G. *Handbook of Material Weathering*, 5th ed.; Elsevier: Amsterdam, The Netherlands, 2013; ISBN 9781895198621.
47. Falaize, S.; Radin, S.; Ducheyne, P. In Vitro Behavior of Silica-Based Xerogels Intended as Controlled Release Carriers. *J. Am. Ceram. Soc.* **1999**, *82*, 969–976. [CrossRef]
48. Kasperek, J.; Verchere, D.; Jacquet, D.; Phillips, N. Analysis of the Corrosion Products on Galvanized Steels by FTIR Spectroscopy. *Mater. Chem. Phys.* **1998**, *56*, 205–213. [CrossRef]
49. Williams, J.; Griffiths, C.; Dunlop, T.; Jewell, E. Improving the Processability of a One-Step Hydrophobic Coating for Hot-Dipped Galvanised Steel for Industrial Applications. *Coatings* **2022**, *12*, 895. [CrossRef]